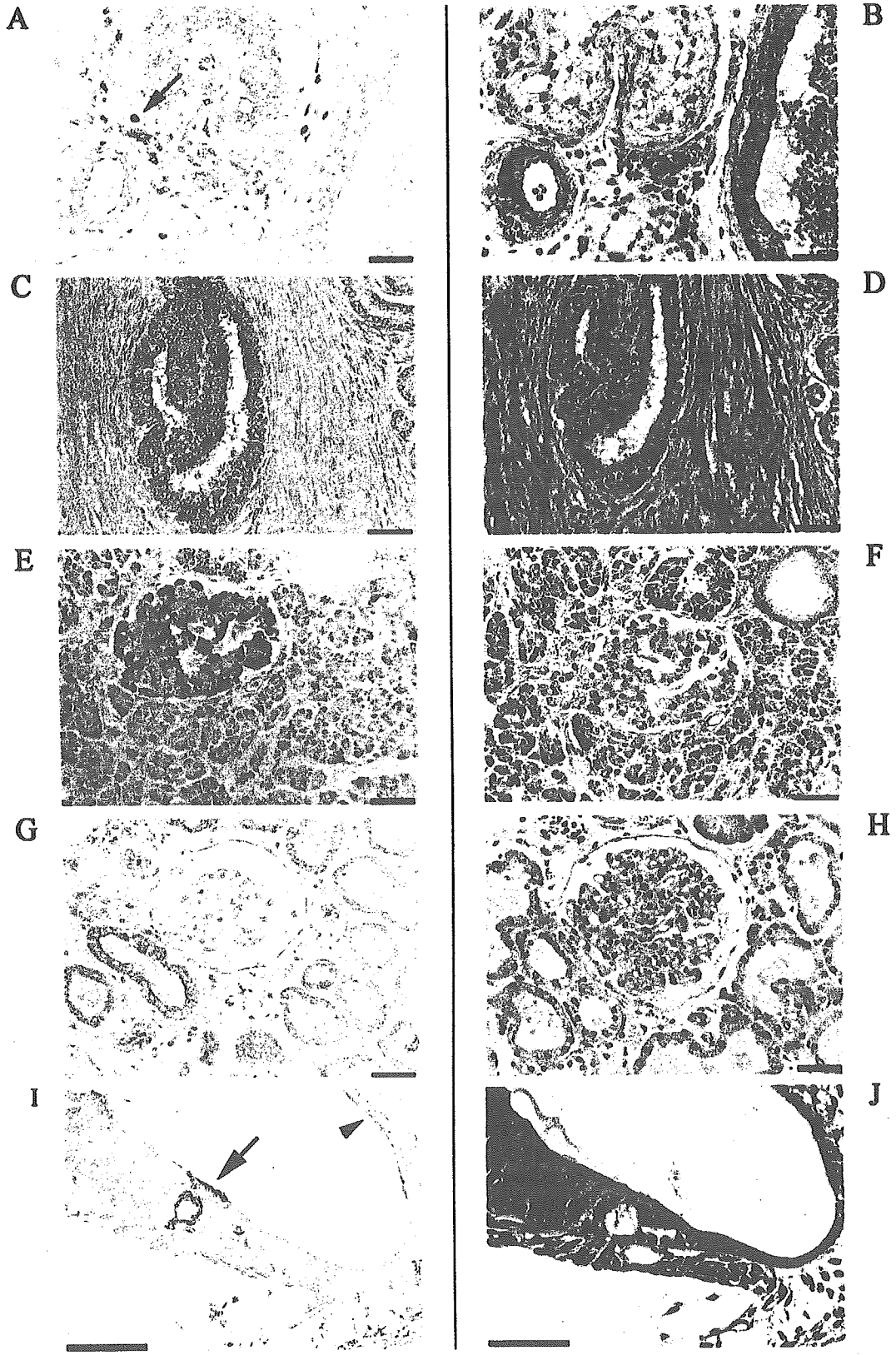
A
B
C
D
E
F
G
H
I
J

tion significantly. Instead, the expression level of *puratrophin-1* mRNA in the patient cerebella appeared slightly low compared with that in control cerebella (fig. 7*A*). On real-time RT-PCR analysis by TaqMan technique, the expression of *puratrophin-1* mRNA in the patient cerebella appeared lower than that in the control samples (fig. 7*B*). The tendency of reduction was seen for both total and short-form *puratrphin-1* mRNAs, although the significance was not proven statistically ($P = .0641$ for total *puratrophin-1* mRNA; $P = .1649$ for short-form *puratrophin-1* mRNA).

The in vitro study with *puratrophin-1* 5′-UTR sequences subcloned into luciferase expression vectors showed significantly reduced luciferase activity; the construct had mutant allele T, and the wild-type construct had allele C (fig. 7*C*). These data suggest that the C→T change in the *puratrophin-1* 5′ UTR could lead to reduced mRNA expression.

Expression of Puratrophin-1 in Control Human and Mouse Tissues and in Brains of Patients with 16q22.1–Linked ADCA

We next examined puratrophin-1 expression by immunohistochemistry using rabbit polyclonal Prtrhn1-Abs. Puratrophin-1 expression was seen in many control human tissues and mouse cochlea (fig. 8). Interestingly, puratrophin-1 expression was commonly seen in epithelial cells, such as epithelial cells in the human testis and hair cells in the mouse cochlea. As far as we examined in human tissues, the strength of immunoreactivity correlated with the mRNA expression level revealed by RT-PCR experiments (fig. 6).

In control human brains, both full-length and short-form puratrophin-1 was expressed faithfully in various neurons but most strongly in Purkinje cells (fig. 9*A*). In chromosome 16q22.1–linked ADCA brains, a striking difference was noted: the presence of microscopic aggregates of puratrophin-1 in the cytoplasm of Purkinje cells (fig. 9*B*). These aggregates were detected with all Prtrhn1-Abs, which indicates that full-length puratrophin-1 and short-form puratrophin-1 were both involved in the aggregate. On the other hand, puratrophin-1 aggregates were not obvious in neurons other than Purkinje cells. The finding of puratrophin-1 aggregates was specific to chromosome 16q22.1–linked ADCA brains, since the aggregates were not seen in other diseases showing degeneration of Purkinje cells, such as SCA6 or MSA.

We next examined the expression of G58K and of the α- and β-spectrin on control and chromosome 16q22.1–linked ADCA brains. Whereas G58K and spectrin were homogeneously stained in control brains (fig. 9*C* and 9*E*), these proteins both formed aggregation within the Purkinje cell of chromosome 16q22.1–linked ADCA brains (fig. 9*D* and 9*F*). This further suggests that formation of puratrophin-1 aggregates is abnormal and associates with disturbances of Golgi apparatus and spectrin.

Discussion

The single-nucleotide C→T substitution in the 5′ UTR of the *puratrophin-1* gene is strongly associated with chromosome 16q22.1–linked ADCA, as evidenced by the following three points. First, this single-nucleotide change was the only specific difference detected in patients, as far as we screened all exons and intron-exon boundaries of the 21 annotated genes lying within the founder chromosome. The change completely segregated with the disease in 52 unrelated families that originated in all sections of Japan, whereas such a change was not seen in 1,000 control chromosomes. We also screened for genomic rearrangement by Southern-blot analysis, but we did not observe any changes. Second, the C→T change was not a mere polymorphism present in the founder chromosome, since it resulted in reduced expression in the in vitro luciferase assay. Consistently, tendency for reduction in mRNA expression was seen in the cerebellum of chromosome 16q22.1–linked ADCA. Third, puratrophin-1 was aggregated in the major target neuron (i.e., the Purkinje cell) of chromosome 16q22.1–linked ADCA. The Golgi-apparatus membrane protein (G58K) and spectrin, both important cytoskeletal proteins, were also aggregated. Since aggregation of mutated protein is a common feature of many neurodegenerative disorders (Ross and Poirier 2004), a single-nucleotide change in the 5′ UTR in the *puratrophin-1* gene appears to be the mutation that causes chromosome 16q22.1–linked ADCA. Most mutations that cause ADCAs reside in genes encoding proteins whose functions are not well understood, except for the α1A-calcium channel ($Ca_v2.1$) for SCA6 (Zhuchenko et al. 1997), PKCγ for

Figure 8 Expression of puratrophin-1 in control human and mouse tissues. *A* and *B*, Human testis. *C* and *D*, Human prostate gland. *E* and *F*, Human pancreas. *G* and *H*, Human kidney. *I* and *J*, Mouse cochlea. *A*, *C*, *E*, *G*, and *I*, Immunohistochemical analysis with use of the polyclonal anti–puratrophin-1 antibody SV01. *B*, *D*, *F*, *H*, and *J*, Hematoxylin and eosin stain of the section adjacent to that shown in *A*, *C*, *E*, *G*, and *I*, respectively. Puratrophin-1 is expressed in many tissues, with varying strength. In particular, Leydig cells in the testis (*arrow* in *A*), epithelial cells in the prostate gland (*C*), and Langerhans islet in the pancreas (*E*) showed strong immunoreactivity. Immunoreactivity in the kidney was weak (*G*). Expression in the cochlea was particularly intense at the sensory hairlets (*arrow* in *I*). Hair cells of the stria vascularis also showed immunoreactivity (*arrowhead* in *I*). All scale bars = 50 μm.

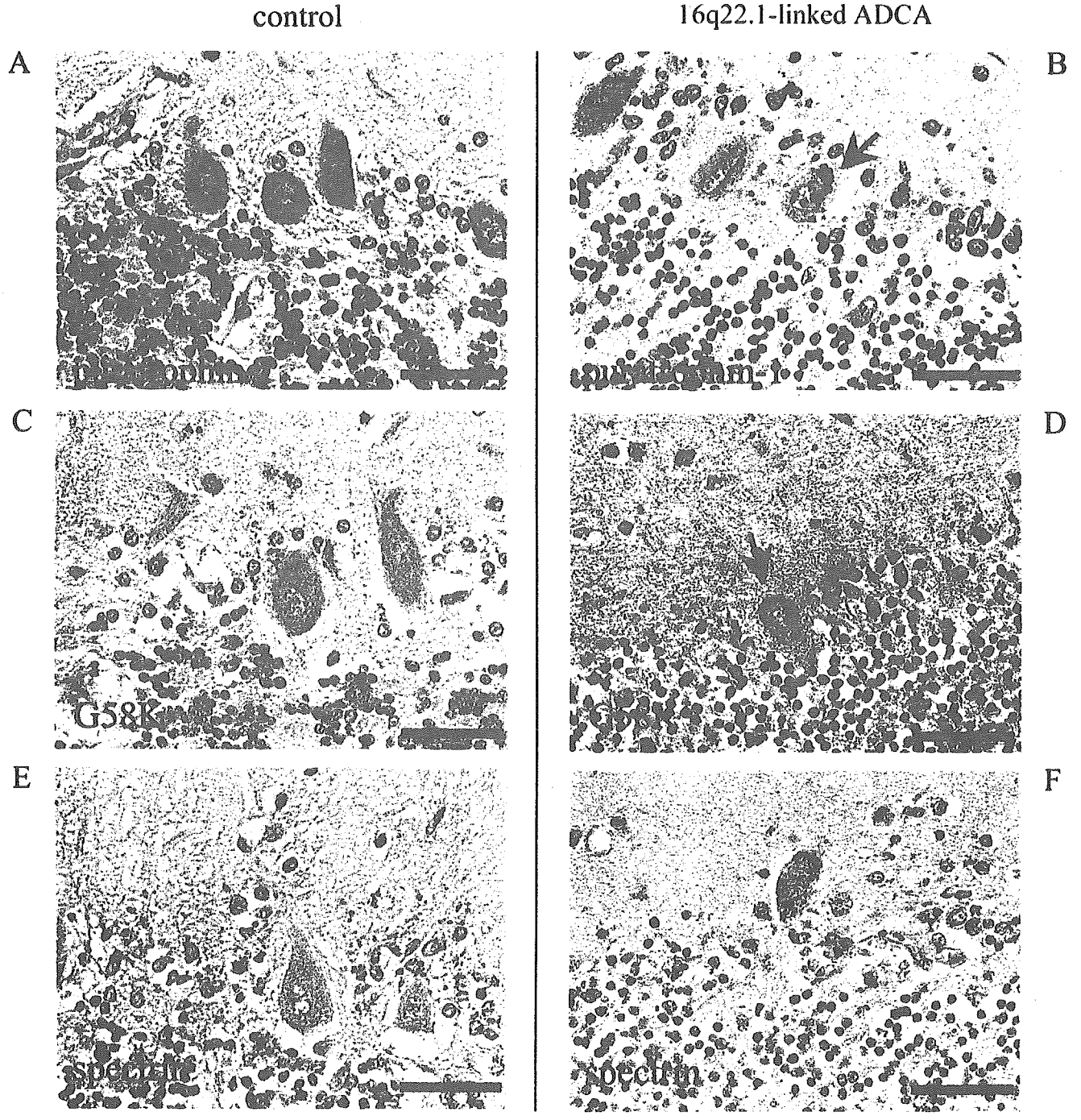

Figure 9 Immunohistochemical analysis of puratrophin-1, Golgi-apparatus membrane protein (G58K), and spectrin in control cells and samples from a patient's cerebellum. *A*, Puratrophin-1 expression in the cell body of Purkinje cells, visualized with use of rabbit polyclonal anti–puratrophin-1 antibody (FL01). *B*, With use of same antibody FL01, aggregation of puratrophin-1 (*arrow*), seen in a Purkinje cell of a brain affected with chromosome 16q22.1–linked ADCA. *C*, G58K expression, seen diffusely in the cell body of control Purkinje cells. *D*, G58K aggregation (*arrow*), morphologically quite similar to the puratrophin-1 aggregate, seen in a patient's Purkinje cell. *E*, Spectrin expression, seen in the cell body of a control Purkinje cell. *F*, Spectrin aggregation in a patient's Purkinje cell. All scale bars = 50 μm.

SCA14 (Chen et al. 2003), TATA-binding protein for SCA17 (Koide et al. 1999), and FGF14 for ADCA with FGF14 mutation (van Swieten et al. 2003). Puratrophin-1 is the first known protein related to intracellular signaling and cytoskeleton that is associated with ADCA. Our preliminary results suggest that the frequency of chromosome 16q22.1–linked ADCA is relatively high, since it was ranked the third most frequent ADCA in Japan, after MJD/SCA3 and SCA6. Since chromosome 16q22.1–linked ADCA had a strong founder effect, it will be important to clarify whether this specific C→T change is seen in other ethnic groups. Particularly, it is extremely important to clarify whether original patients with SCA4 reported from North American and German populations harbor mutation within the *puratrophin-1* gene (Flanigan et al. 1996; Hellenbroich et al. 2003).

A heterozygous, single-nucleotide substitution in the 5′ UTR that is associated with aggregation of the gene product is a unique feature as a cause of human disease. Generally, a single-nucleotide substitution in the 5′ UTR may result in expression of aberrant mRNA, abnormal trafficking of mutant transcripts due to conformational changes, or reduced transcription of mRNA, as in β thalassemia intermedia (Sgourou et al. 2004). In the present study, no aberrant transcripts were cloned from patient brains. Instead, the result from the in vitro study suggested that the transcription efficiency could be reduced significantly by the C→T substitution in the 5′ UTR of the *puratrophin-1* gene. Consistent with this in vitro finding, levels of *puratrophin-1* mRNA tended to be lower in cerebella of patients with 16q22.1-linked ADCA than in those of AD-affected controls. Further studies comprising a larger number of samples that include "neurologically normal" controls will be necessary to confirm that reduced *puratrophin-1* mRNA expression is associated with the C→T change in the 5′ UTR. Although aggregations of mutated proteins in most neurodegenerative diseases are due to conformational changes produced by amino acid alterations, reduced protein expression may also cause protein aggregation, such as the neurofilament light-chain aggregation in anterior horn cells of patients with amyotrophic lateral sclerosis (ALS) (Bergeron et al. 1994). It is currently not known how the C→T change in the *puratrophin-1* gene leads to puratrophin-1 aggregation. However, it is possible that alteration in the stoichiometry or changes in the protein stability, observed in neurofilament proteins in ALS (Ge et al. 2003), also exist for puratrophin-1 in chromosome 16q22.1–linked ADCA. In addition, it should be noted that since reduction of *puratrophin-1* mRNA levels in patient cerebella was small, that may not be a sufficient explanation of the formation of aggregation. It will be important to assess the *puratrophin-1* mRNA levels specifically in Purkinje cells, where the protein aggregates.

Puratrophin-1 is a novel protein with four important domains: the spectrin repeat, CRAL/TRIO, Rho GEF/DH, and PH domains. Therefore, the *puratrophin-1* gene would be the fifth gene that encodes Rho GEF protein to be associated with human disease, after the *FGD1GEF* gene for faciogenital dysplasia (Pasteris et al. 1994), the *ARHGEF6* gene for X-linked nonsyndromic mental retardation (Kutsche et al. 2000), the *ARHGEF10* gene for autosomal dominant neuropathy with thin myelinated fibers (Verhoeven et al. 2003), and the *ALS2* gene for the autosomal recessive juvenile motor neuron disease ALS2 (Hadano et al. 2001; Yang et al. 2001). GEFs exert diverse functions in intracellular-membrane trafficking and microtubule dynamics and ultimately regulate numerous cellular responses—such as proliferation, differentiation, and movement—by activating small G-protein GTPases (Rossman et al. 2005). Although Rho GEF/DH and PH domains are typical for Rho GEF proteins, the presence of a spectrin repeat suggests that puratrophin-1 could be targeted to the Golgi-apparatus membrane, where it may regulate certain membrane dynamics through modulating actin (Godi et al. 1998; Lemmon et al. 2002). The CRAL/TRIO domain is implicated in the nerve growth factor (NGF) pathway that leads to neurite outgrowth through activating Rho G (Estrach et al. 2002), which indicates that puratrophin-1 may also have a role in cell differentiation signaling through NGF. In the present study, we showed that the Golgi-apparatus membrane protein and spectrin both form aggregation in the Purkinje cells of patient brains, which strongly supports the hypothesis that puratrophin-1 indeed interacts with these essential cytoskeletons. Formation of these aggregations, which seems to be a new phenomenon implicated in pathogenesis of human disease, could be deleterious for cells, since Golgi-apparatus membrane proteins and spectrin are important in maintaining cellular architecture, as noted for autosomal dominant polycystic kidney diseases (Charron et al. 2000). In addition, it also seems rational to speculate that disturbance of puratrophin-1 may affect Purkinje-cell morphology and eventually cause the peculiar Purkinje-cell atrophy that characterizes chromosome 16q22.1–linked ADCA, since Rho GEFs are implicated particularly in neural morphogenesis and connectivity by regulating actin dynamics (Godi et al. 1998).

Finally, the association of progressive hearing impairment in patients with chromosome 16q22.1–linked ADCA may suggest a role of puratrophin-1 in hearing. As far as we were able to examine by auditory tests, 42.8% of study families had hearing impairment. Audiometric configurations showing mid-frequency U-shaped or flat-shaped pattern also suggested that the hearing impairment of these patients was not a simple age-related hearing loss. However, it should be noted

that some families had moderate hearing impairment, whereas other families had only mild hearing impairment, which may indicate the presence of other modifying genetic factors for this phenotype. Further clinical analyses with use of detailed auditory tests are needed to ascertain how strongly hearing impairment is associated with ataxia. If hearing impairment is confirmed as being complicated by chromosome 16q22.1–linked ADCA, puratrophin-1 will be the first deafness/hearing-impairment protein related to Rho GEF. Since mutations in the γ-actin gene (*ACTG1*; DFN20/26) (Zhu et al. 2003), genes coding proteins that interact with actin (e.g., the myosins espin and harmonin), or a gene coding proteins that coordinate actin polymerization (Mburu et al. 2003) are known to cause deafness, it is possible that puratrophin-1 disruption causes hearing impairment by disturbing actin dynamics in the cochlea. In support of this hypothesis, expression of puratrophin-1 was seen in mouse cochlear hair cells, in which actin is also expressed (Mburu et al. 2003). Rho GTPases are also important regulators of actin cytoskeleton in stereocilia development, which is crucial for auditory transduction (Kollmar 2001). We hypothesize that the *puratrophin-1* gene mutation ultimately causes hearing impairment by dysregulation of actin in the cochlea. Further studies, such as targeted disruption of puratrophin-1 in mouse, will be important for clarifying whether puratrophin-1 has a role in hearing.

In summary, we have identified that a single-nucleotide C→T substitution in the 5′ UTR of the gene *puratrophin-1* is strongly associated with chromosome 16q22.1–linked ADCA. If patients with SCA4 are found to harbor mutations in this gene, it would suggest that the chromosome 16q22.1–linked ADCA in Japan is allelic with SCA4. Identification of the mechanism of puratrophin-1 expression, the upstream signaling cascade that activates puratrophin-1, and the actual Rho GTPase activated by puratrophin-1 would be the next key steps for understanding the molecular mechanisms that underlie cellular degeneration of chromosome 16q22.1–linked ADCA and hearing impairment.

Acknowledgments

We thank the doctors who participated in this work by recruiting families with chromosome 16q22.1–linked ADCA: Drs. Hidenao Sasaki, Department of Neurology, Graduate School, Hokkaido University; Masashi Aoki, Department of Neurology, Graduate School, Tohoku University; Yoshihisa Takiyama, Department of Neurology, Jichi Medical School; Kazuo Yoshizawa, National Mito Hospital; Kazuko Mitani and Yu-ichi Fumimura, Department of Neurology, Tokyo Metropolitan Geriatric Hospital; Hirohiko Murakami, Department of Neurology, Tokyo Women's Medical School; Satoshi Orimo, Department of Neurology, Kanto Central Hospital; Souichiro Mochio, Department of Neurology, Jikei Medical School, The Third Hospital; Kunihiro Yoshida, Department of Clinical Genetics, Shinshu University; Isao Sahashi, Fourth Department of Internal Medicine, Aichi Medical University; Masanori Nakagawa, Department of Neurology, Kyoto Prefectural Medical College; Akihumi Goto, Department of Neurology, Nagasaki Medical Center of Neurology; Hideki Kida, Kida Hospital; Eiichiro Uyama, Department of Neurology, Kumamoto University of Medicine; Jun Goto and Shoji Tsuji, Department of Neurology, Graduate School, University of Tokyo; and Miho Murata and Ichiro Kanazawa, National Center of Neurology and Psychiatry, Ministry of Health, Labor and Welfare. For human and mouse control specimens, we also thank Professors Morio Koike, Department of Pathology, and Ken Kitamura, Department of Audio-Vestibular Neuroscience, Graduate School, Tokyo Medical and Dental University. We thank Ms. Iku Sudo and Ms. Minori Kono for technical assistance. We deeply acknowledge Professors Ichiro Kanazawa, Director of National Center of Neurology and Psychiatry, Ministry of Health, Labor and Welfare, and Shoji Tsuji, Department of Neurology, Graduate School, University of Tokyo, for supporting this study. This study was supported by Grant-in-Aids for Scientific Research on Priority Areas—Advanced Brain Science Project—from Ministry of Education, Culture, Sports, Science and Technology, Japan (to K.I. and H.M.), as well as grants from Research on Intractable Disorders (to H.M.) and from Human Genome and Regenerative Medicine, Ministry of Health, Labor and Welfare, Japan (to K.I. and H.M.).

Web Resources

Accession numbers and URLs for data presented herein are as follows:

Celera Discovery System, http://www.celeradiscoverysystem.com/index.cfm (for candidate genes)

Ensembl, http://www.ensembl.org/ (for genetic map, genomic sequences, ESTs, and 21 candidate genes, including *Q9H7K4* and *SLC9A5*)

GenBank, http://www.ncbi.nlm.nih.gov/Genbank/ (for microsatellite DNA markers *GGAA10* [accession number AB13610], TTCC01 [accession number AB13611], *TA001* [accession number AB13612], *GA001* [accession number AB197662], and *AAT01* [accession number AB13613] and full-length and short-form *puratrophin-1* mRNAs [accession numbers AB197663 and AB197664])

NCBI, http://www.ncbi.nlm.nih.gov/ (for DKFZP434I216 [accession numbers BC054486 and AK024475])

Online Mendelian Inheritance in Man (OMIM), http://www.ncbi.nlm.nih.gov/Omim/ (for 16q-linked ADCA type III, or SCA4)

The Hereditary Hearing Loss Homepage, http://webhost.ua.ac.be/hhh/

UniGene, http://www.ncbi.nlm.nih.gov/UniGene/ (for candidate genes and ESTs)

References

Bergeron C, Beric-Maskarel K, Muntasser S, Weyer L, Somerville M, Percy ME (1994) Neurofilament light and polyaden-

ylated mRNA levels are decreased in amyotrophic lateral sclerosis motor neurons. J Neuropathol Exp Neurol 53:221–230

Charron AJ, Bacallao RL, Wandinger-Ness A (2000) ADPKD: a human disease altering Golgi function and basolateral exocytosis in renal epithelia. Traffic 1:675–686

Chen D-H, Brkanac Z, Verlinde CLMJ, Tan X-J, Bylenok L, Nochlin D, Matsushita M, Lipe H, Wolff J, Fernandez M, Cimino PJ, Bird TD, Raskind WH (2003) Missense mutations in the regulatory domain of PKCγ: a new mechanism for dominant nonepisodic cerebellar ataxia. Am J Hum Genet 72:839–849

Estrach S, Schmidt S, Diriong S, Penna A, Blangy A, Fort P, Debant A (2002) The human Rho-GEF trio and its target GTPase RhoG are involved in the NGF pathway, leading to neurite outgrowth. Curr Biol 12:307–312

Flanigan K, Gardner K, Alderson K, Galster B, Otterud B, Leppert MF, Kaplan C, Ptacek LJ (1996) Autosomal dominant spinocerebellar ataxia with sensory axonal neuropathy (SCA4): clinical description and genetic localization to chromosome 16q22.1. Am J Hum Genet 59:392–399

Fucini RV, Navarrete A, Vadakkan C, Lacomis L, Erdjument-Bromage H, Tempst P, Stamnes M (2000) Activated ADP-ribosylation factor assembles distinct pools of actin on Golgi membranes. J Biol Chem 275:18824–18829

Ge WW, Leystra-Lantz C, Wen W, Strong MJ (2003) Selective loss of trans-acting instability determinants of neurofilament mRNA in amyotrophic lateral sclerosis spinal cord. J Biol Chem 278:26558–26563

Godi A, Santone I, Pertile P, Devarajan P, Stabach PR, Morrow JS, DiTullio G, Polishchuk R, Petrucci TC, Luini A, DeMatteis MA (1998) ADP ribosylation factor regulates spectrin binding to the Golgi complex. Proc Natl Acad Sci USA 95: 8607–8612

Graham DI, Lantos PL (eds) (2002) Greenfield's neuropathology, 7th ed. Arnold, London

Hadano S, Hand CK, Osuga H, Yanagisawa Y, Otomo A, Devon RS, Miyamoto N, Showguchi-Miyata J, Okada Y, Singaraja R, Figlewicz DA, Kwiatkowski T, Hosler BA, Sagie T, Skaug J, Nasir J, Brown RH Jr, Scherer SW, Rouleau GA, Hayden MR, Ikeda JE (2001) A gene encoding a putative GTPase regulator is mutated in familial amyotrophic lateral sclerosis 2. Nat Genet 29:166–173

Harding AE (1982) The clinical features and classification of the late onset autosomal dominant cerebellar ataxias: a study of 11 families, including descendants of "Drew family of Walworth." Brain 105:1–28

Hellenbroich Y, Bubel S, Pawlack H, Opitz S, Vieregge P, Schwinger E, Zuhlke C (2003) Refinement of the spinocerebellar ataxia type 4 locus in a large German family and exclusion of CAG repeat expansion in this region. J Neurol 250:668–671

Hirano R, Takashima H, Okubo R, Tajima K, Okamoto Y, Ishida S, Tsuruta K, Arisato T, Arata H, Nakagawa M, Osame M, Arimura K (2004) Fine mapping of 16q-linked autosomal dominant cerebellar ataxia type III in Japanese families. Neurogenetics 5:215–221

Holmes SE, O'Hearn EE, McInnis MG, Gorelick-Feldman DA, Kleiderlein JJ, Callahan C, Kwak NG, Ingersoll-Ashworth RG, Sherr M, Sumner AJ, Sharp AH, Ananth U, Seltzer WK, Boss MA, Vieria-Saecker AM, Epplen JT, Riess O, Ross CA, Margolis RL (1999) Expansion of a novel CAG trinucleotide repeat in the 5′ region of PPP2R2B is associated with SCA12. Nat Genet 23:391–392

Hughes CP, Berg L, Danziger WL, Coben LA, Martin RL (1982) A new clinical scale for the staging of dementia. Br J Psychiatry 140:566–572

Ishikawa K, Fujigasaki H, Saegusa H, Ohwada K, Fujita T, Iwamoto H, Komatsuzaki Y, Toru S, Toriyama H, Watanabe M, Ohkoshi N, Shoji S, Kanazawa I, Tanabe T, Mizusawa H (1999) Abundant expression and cytoplasmic aggregation of α1A voltage-dependent calcium channel protein associated with neurodegeneration in spinocerebellar ataxia type 6. Hum Mol Genet 8:1185–1193

Ishikawa K, Nagaoka U, Takashima M, Yoshizawa K, Yoshizawa T, Ishikawa M, Yamawaki T, Shoji S, Mizusawa H (2000) A gene on SCA4 locus causes dominantly-inherited pure cerebellar ataxia. Neurology 54:1971–1975

Ishikawa K, Tanaka H, Saito M, Ohkoshi N, Fujita T, Yoshizawa K, Ikeuchi T, Watanabe M, Hayashi A, Takiyama Y, Nishizawa M, Nakano I, Matsubayashi K, Miwa M, Shoji S, Kanazawa I, Tsuji S, Mizusawa H (1997) Japanese families with autosomal dominant pure cerebellar ataxia map to chromosome 19p13.1-p13.2 and are strongly associated with mild CAG expansions in the spinocerebellar ataxia type 6 gene in chromosome 19p13.1. Am J Hum Genet 61:336–346

Kobayashi K, Nakahori Y, Miyake M, Matsumura K, Kondo-Iida E, Nomura Y, Segawa M, Yoshioka M, Saito K, Osawa M, Hamano K, Sakakihara Y, Nonaka I, Nakagome Y, Kanazawa I, Nakamura Y, Tokunaga K, Toda T (1998) An ancient retrotransposal insertion causes Fukuyama-type congenital muscular dystrophy. Nature 394:388–392

Koide R, Kobayashi S, Shimohata T, Ikeuchi T, Maruyama M, Saito M, Yamada M, Takahashi H, Tsuji S (1999) A neurological disease caused by an expanded CAG trinucleotide repeat in the TATA-binding protein gene: a new polyglutamine disease? Hum Mol Genet 8:2047–2053

Kollmar R (2001) Who does the hair cell's 'do? Rho GTPases and hair-bundle morphogenesis. Curr Opin Neurobiol 9:394–398

Koob MD, Moseley ML, Schut LJ, Benzow KA, Bird TD, Day JW, Ranum LP (1999) An untranslated CTG expansion causes a novel form of spinocerebellar ataxia (SCA8). Nat Genet 21:379–384

Kutsche K, Yntema H, Brandt A, Jantke I, Nothwang HG, Orth U, Boavida MG, David D, Chelly J, Fryns J-P, Moraine C, Ropers H-H, Hamel BCJ, van Bokhoven H, Gal A (2000) Mutations in *ARHGEF6*, encoding a guanine nucleotide exchange factor for Rho GTPases, in patients with X-linked mental retardation. Nat Genet 26:247–250

Lemmon MA, Ferguson KM, Abrams CS (2002) Pleckstrin homology domains and cytoskeleton. FEBS Lett 513:71–76

Li M, Ishikawa K, Toru S, Tomimitsu H, Takashima M, Goto J, Takiyama Y, Sasaki H, Imoto I, Inazawa J, Toda T, Kanazawa I, Mizusawa H (2003) Physical map and haplotype analysis of 16q-linked autosomal dominant cerebellar ataxia (ADCA) type III in Japan. J Hum Genet 48:111–118

Margolis RL (2002) The spinocerebellar ataxias: order emerges from chaos. Curr Neurol Neurosci Rep 2:447–456

Matsuura T, Yamagata T, Burgess DL, Rasmussen A, Grewal RP, Watase K, Khajavi M, McCall AE, Davis CF, Zu L, Achari M, Pulst SM, Alonso E, Noebels JL, Nelson DL, Zoghbi HY, Ashizawa T (2000) Large expansion of the ATTCT pentanucleotide repeat in spinocerebellar ataxia type 10. Nat Genet 26:191–194

Mburu P, Mustapha M, Varela A, Weil D, El-Amraoui A, Holme RH, Rump A, Hardisty RE, Blanchard S, Coimbra RS, Perfettini I, Parkinson N, Mallon A-M, Glenister P, Rogers MJ, Paige AJ, Moir L, Clay J, Rosenthal A, Liu XZ, Blanco G, Steel KP, Petit C, Brown SDM (2003) Defects in whirlin, a PDZ domain molecule involved in stereocilia elongation, cause deafness in the whirler mouse and families with DFNB31. Nat Genet 34:421–428

Owada K, Ishikawa K, Toru S, Ishida G, Gomyoda M, Tao O, Noguchi Y, Kitamura K, Kondo I, Noguchi E, Arinami T, Mizusawa H. A clinical, genetic and neuropathologic study in a family with 16q-linked ADCA type III. Neurology (in press)

Pasteris NG, Cadle A, Logie LJ, Porteous ME, Schwartz CE, Stevenson RE, Glover TW, Wilroy RS, Gorski JL (1994) Isolation and characterization of the faciogenital dysplasia (Aarskog-Scott syndrome) gene: a putative Rho/Rac guanine nucleotide exchange factor. Cell 79:669–678

Ross CA, Poirier MA (2004) Protein aggregation and neurodegenerative disease. Nat Med Suppl 10:S10–S17

Rossman KL, Der CJ, Sondek J (2005) GEF means go: turning on RHO GTPases with guanine nucleotide-exchange factors. Nat Rev Mol Cell Biol 6:167–180

Sasaki H, Yabe I, Tashiro K (2003) The hereditary spinocerebellar ataxias in Japan. Cytogenet Genome Res 100:198–205

Sgourou A, Routledge S, Antoniou M, Papachatzopoulou A, Psiouri L, Athanassiadou A (2004) Thalassaemia mutations within the 5′ UTR of the human β-globin gene disrupt transcription. Br J Haematol 124:828–835

Stevanin G, Bouslam N, Thobois S, Azzedine H, Ravaux L, Boland A, Schalling M, Broussole E, Durr A, Brice A (2004) Spinocerebellar ataxia with sensory neuropathy (SCA25) maps to chromosome 2p. Ann Neurol 55:97–104

Stevanin G, Durr A, Brice A (2000) Clinical and molecular advances in autosomal dominant cerebellar ataxias: from genotype to phenotype and physiopathology. Eur J Hum Genet 8:4–18

Tsuiki T, Sasamori S, Minami Y, Ichinohe T, Murai K, Murai S, Kawashima H (2002) [Age effect on hearing: a study on Japanese.] Audiol Japan 45:241–250

Tsunemi T, Saegusa H, Ishikawa K, Nagayama S, Murakoshi T, Mizusawa H, Tanabe T (2002) Novel $Ca_v2.1$ splice variants isolated from Purkinje cells do not generate P-type Ca^{2+} current. J Biol Chem 277:7214–7221

van Swieten JC, Brusse E, de Graaf BM, Krieger E, van de Graaf R, de Koning I, Maat-Kievit A, Leegwater P, Dooijes D, Oostra BA, Heutink P (2003) A mutation in the fibroblast growth factor 14 gene is associated with autosomal dominant cerebellar ataxia. Am J Hum Genet 72:191–199 (erratum 72:1078)

Verhoeven K, De Jonghe P, Van de Putte T, Nelis E, Zwijsen A, Verpoorten N, De Vriendt E, Jacobs A, Van Gerwen V, Francis A, Ceuterick C, Huylebroeck D, Timmerman V (2003) Slowed conduction and thin myelination of peripheral nerves associated with mutant Rho guanine-nucleotide exchange factor 10. Am J Hum Genet 73:926–932

Yang Y, Hentati A, Deng HX, Dabbagh O, Sasaki T, Hirano M, Hung WY, Ouahchi K, Yan J, Azim AC, Cole N, Gascon G, Yagmour A, Ben-Hamida M, Pericak-Vance M, Hentati F, Siddique T (2001) The gene encoding alsin, a protein with three guanine-nucleotide exchange factor domains, is mutated in a form of recessive amyotrophic lateral sclerosis. Nat Genet 29:160–165

Yu GY, Howell MJ, Roller MJ, Xie TD, Gomez CM (2005) Spinocerebellar ataxia type 26 maps to chromosome 19p13.3 adjacent to SCA6. Ann Neurol 57:349–354

Zhu M, Yang T, Wei S, DeWan AT, Morell RJ, Elfenbein JL, Fisher RA, Leal SM, Smith RJH, Friderici KH (2003) Mutations in the γ-actin gene (*ACTG1*) are associated with dominant progressive deafness (DFNA20/26). Am J Hum Genet 73:1082–1091

Zhuchenko O, Bailey J, Bonnen P, Ashizawa T, Stockton DW, Amos C, Dobyns WB, Subramony SH, Zoghbi HY, Lee CC (1997) Autosomal dominant cerebellar ataxia (SCA6) associated with small polyglutamine expansions in the α1A-voltage-dependent calcium channel. Nat Genet 15:62–69

ELSEVIER

Atherosclerosis 179 (2005) 345–351

ATHEROSCLEROSIS

www.elsevier.com/locate/atherosclerosis

Aortic pulse wave velocity and the degree of atherosclerosis in the elderly: a pathological study based on 304 autopsy cases

Motoji Sawabe[a,*], Ryutaro Takahashi[b,c], Satoru Matsushita[b], Toshio Ozawa[b], Tomio Arai[a], Akihiko Hamamatsu[a], Ken-ichi Nakahara[b], Kouji Chida[b], Hiroshi Yamanouchi[b], Shigeo Murayama[d], Noriko Tanaka[e]

[a] *Department of Pathology, Tokyo Metropolitan Geriatric Hospital, 35-2 Sakae-cho, Itabashi, Tokyo 173-0015, Japan*
[b] *Department of Internal Medicine, Tokyo Metropolitan Geriatric Hospital, Tokyo, Japan*
[c] *Human Care Research Group, Tokyo Metropolitan Institute of Gerontology, Tokyo, Japan*
[d] *Geriatric Neuroscience Research Group, Tokyo Metropolitan Institute of Gerontology, Tokyo, Japan*
[e] *Department of Biostatistics, Graduate School of Medicine, Tokyo University, Tokyo, Japan*

Received 19 December 2003; received in revised form 15 September 2004; accepted 30 September 2004
Available online 13 December 2004

Abstract

Introduction: Studies examining the correlation between aortic pulse wave velocity (PWV) and atherosclerosis have reported conflicting results. The present paper verifies this correlation by conducting autopsy examination of elderly subjects.
Methods: A total of 3456 PWV examinations had been performed on 1538 elderly people, as a part of routine physical check-up. During long-term follow-up, many of these subjects died, and autopsy study could be conducted on 304 of these subjects. The average age at death of the subjects was 83 years and the male: female ratio was 6:5. The pathological atherosclerotic index (PAI) was defined as the average pathological degree of atherosclerosis in eight large arteries, including aorta.
Results: Significant positive correlations were observed between the age and PWV ($\gamma = 0.273$, $P < 0.001$), and between the systolic blood pressure and PWV ($\gamma = 0.478$, $P < 0.001$). There was a significantly positive correlation between the aortic atherosclerotic degree and mean PWV ($\rho = 0.239$, $P < 0.005$), and between the PAI and mean PWV ($\gamma = 0.323$, $P < 0.001$). The partial regression coefficient between the PAI and mean PWV was 0.209, after adjusting for the mean systolic blood pressure and age at death.
Conclusion: The present study proved a weak correlation between the PWV and the pathologically verified degree of the aortic and systemic atherosclerosis.

Keywords: Aging; Aorta; Atherosclerosis; Compliance; Elderly; Human; Pulse wave velocity

1. Introduction

The pulse wave velocity (PWV) is a marker of the elasticity of elastic or muscular arteries (aorta and its major branches), and reflects mainly the mechanical properties of the arterial wall. Diffuse sclerotic changes of the arterial wall observed in elderly or hypertensive cases increase the arterial stiffness. Meanwhile, the atherosclerosis is frequently associated with aging and hypertension. Although the atherosclerosis is initially localized to the intima, it finally affects the entire arterial lumen and results in medial destruction and fibrosis, and intimal calcification. Thus, the diffuse atherosclerosis likely causes the increase of arterial stiffness, especially in the advanced stage. Conflicting results have been reported on the correlation between the arterial stiffness and the severity of atherosclerosis. Avolio et al. reported that the PWV correlated well with the age in a northern Chinese community,

Abbreviations: BAI, brain atherosclerotic index; CSI, coronary stenotic index; PAI, pathological atherosclerotic index; PWV, pulse wave velocity

* Corresponding author. Tel.: +81 3 3964 1141; fax: +81 3 3964 1982.
E-mail address: sawabe@tmig.or.jp (M. Sawabe).

0021-9150/$ – see front matter © 2004 Elsevier Ireland Ltd. All rights reserved.
doi:10.1016/j.atherosclerosis.2004.09.023

known for its low serum cholesterol level and low prevalence of atherosclerosis in its population, and argued that atherosclerosis is therefore probably not the dominant factor responsible for the increase of PWV with aging [1,2]. Recent studies have reported that the PWV is high in cases with atherosclerotic complications, such as those with coronary heart disease and cerebrovascular disease, and that it is an important risk factor of cardiovascular mortality and primary coronary events, concluding that the PWV may indeed be a clinical marker of atherosclerosis [3–6]. Several trials of radiological evaluation of atherosclerosis by ultrasound, CT and MRI have been reported [7,8], and a significant correlation has been described between the PWV and surrogate radiological markers of atherosclerosis, such as the carotid artery intima-media thickness and plaques in the carotid arteries and aorta [9,10]. Since the degree of atherosclerosis differs from artery to artery, and even within the same artery, it is uncertain how reliably these radiological markers would reflect the degree of aortic or systemic atherosclerosis. Thus, the definitive and most direct assessment method of atherosclerosis still remains the pathological examination of resected arterial specimens or autopsy materials. However, no reports are available in the English medical literature that provides evidence of a positive correlation between PWV and the pathologically verified degree of atherosclerosis.

We performed PWV measurements as a part of routine physical check-up in a large number of elderly people and reported the results in a previous publication [11]. Many of these subjects died during long-term follow-up, and autopsy study could be conducted on some of them at our hospital. The present paper presents the results of a pathological study on the correlation between PWV and the severity of atherosclerosis, based on 304 elderly autopsy examinations.

2. Patients and methods

2.1. Patients

A total of 3456 PWV examinations were performed on 1538 unselected residents of Itabashi Home for the Aged, Tokyo, as a part of routine physical check-up between 1984 and 1996. During this period and subsequent long-term follow-up, some of these subjects died, and autopsy could be conducted in 304 cases among these residents at the Department of Pathology of Tokyo Metropolitan Geriatric Hospital, Tokyo, Japan. Both Itabashi Home for the Aged and Tokyo Metropolitan Geriatric Hospital are located in the same campus. The autopsy cases were composed of 165 males and 139 females. The age at death ranged from 67 to 103 years with an average age of 83 years. The most common cause of death was malignant neoplasms (29%), followed by infection (24%) and respiratory insufficiency excluding pneumonia (13%). Myocardial infarction and cerebrovascular disease were the main causes of death in 30 cases (10%) and 27 cases (9%), respectively. Aneurysmal rupture was found in seven cases (2%). Other diseases included gastrointestinal diseases (4%), renal failure (2%), hepatopancreatic diseases (1%), and miscellaneous conditions (6%). No cases of Takayasu's arteritis or Marfan's syndrome were included.

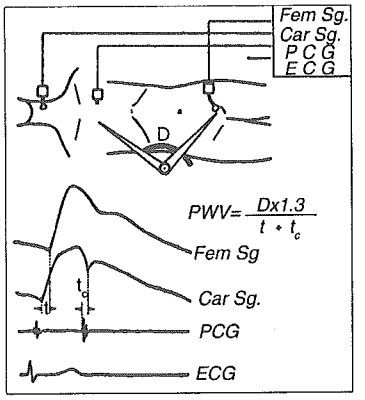

Fig. 1. Schematic diagram of the PWV measurement. Quoted from Figure 3 of the article no. [12] of the reference lists, by Yoshimura et al. by courtesy of the copyright holder. D, distance (in meters) from the second intercostal space at the right sternal edge to the point where the femoral pulse is palpated; 1.3 is a calculated constant of the ratio of the aortic length to D; t, the time interval (second) from the onset of the rapid ascending limb of the carotid pulse wave to that of the femoral pulse wave; t_c, central pulse wave transmission time (second), namely, the time interval from the beginning of the second heart sound to the notch of the carotid pulse wave.

In the present study, the relationship between the results of PWV examination and the clinicopathological findings in these autopsy cases was analyzed.

2.2. Pulse wave velocity

The aortic, carotid-femoral PWV was measured by a tonometric method, using the Automatic Aortic Pulse Wave Velocity Meter (MCG400) manufactured by Fukuda Denshi Co. Ltd., Tokyo. According to Yoshimura's method [12], the PWV was calculated using the following equation: $\mathrm{PWV} = (D \times 1.3)/(t + t_c)$, and the schematic diagram of the PWV examination was shown in Fig. 1. The systolic and diastolic pressures were measured at these examinations. The reproducibility of the PWV measurement was checked by the review of 49 cases in which the PWV was measured twice at 4-month intervals. The correlation coefficient was high ($\gamma = 0.733$, $P < 0.0001$). The average values of the PWV and blood pressure were used for the statistical analyses, when the PWV examinations were repeated in any person.

2.3. Vascular pathology

After en-bloc extirpation of the cervical, mediastinal, retroperitoneal and pelvic organs at autopsy, the large arteries were cut open and fixed in 10% formalin solution. The severity of atherosclerosis was evaluated macroscopically by examination of their inner surfaces, except for the

case of the splenic and superior mesenteric arteries, which were evaluated on cut sections. According to modification of Gore–Tejada's atherosclerotic index [13], the atherosclerosis in the large arteries was semi-quantitatively scored on a scale of 0–8 according to the ratio of the atheroma-occupied area to the entire surface area: negligible (0 point, ratio = 0–1/20), minimal (2 points, 1/20–1/6), mild (4 points, 1/6–1/3), moderate (6 points, 1/3–2/3), and severe (8 points, 2/3–1). The large arteries examined included the common carotid artery, subclavian artery, aorta, splenic artery, superior mesenteric artery, common iliac artery, external iliac artery, and left femoral artery. In the case of bilateral arteries, the average score of the left and right sides was calculated. The term of "atheroma" was used in a broad sense, and it included fatty streaks, fibrous plaques, fibro-fatty plaques, and complicated lesions. It did not include mild diffuse intimal thickening, which is described as the aging phenomenon. Thus, the atherosclerotic changes could be differentiated from the aging changes of the arteries. The Pathological Atherosclerotic Index (PAI) was defined as the average value of the atherosclerotic scores in these eight large arteries. The PAI was calculated in 275 cases in which the atherosclerotic scores of all the eight arteries could be evaluated.

The Coronary Stenotic Index (CSI) was measured by one of the authors (K.C.), as previously reported [14,15]. Intracranial arteries were also semi-quantitatively examined by one of the authors (H.Y.), as previously reported [16]. The Brain Atherosclerotic Index (BAI) was defined as the average of the atherosclerotic scores of five intracranial arteries, including the anterior cerebral arteries, middle cerebral arteries, posterior cerebral arteries, basilar artery and vertebral arteries.

2.4. Statistical analysis

The atherosclerotic scores of individual arteries were compared by Friedman's test. The average values of the PWV and PAI were compared by Student's t-test or Welch's t-test. The atherosclerotic scores of the left- and right-sided arteries were compared by Wilcoxon's rank sum test. The correlations among the PWV, age at death, blood pressure, the atherosclerotic scores of individual arteries, and the PAI were studied by Spearman's rank correlation or Pearson's correlation. The correlation coefficients of Spearman's rank correlation and Pearson's correlation were designated as ρ and γ, respectively. Finally, a meta-regression method was applied to examine whether the changing rate of an individual's PWV was correlated with the PAI. The significance level was set at 0.05. The SAS system for Windows (Version 8.1) and StatView (Version 5.0) (SAS Institute Inc., NC) were used for the statistical analyses. The statistical analyses were performed by two of the authors (N.T. and M.S.).

2.5. Ethical considerations

Written informed consents were obtained from the bereaved family of the patients at the time of autopsy. The use of autopsy materials for medical education and research is generally permitted in accordance with the Act of Post-mortem Examinations of Japan.

3. Results

3.1. Pulse wave velocity

The histogram of the mean PWV showed normal distribution, with a mean (±S.D.) of 9.6 (±1.8) m/s. The mean PWV ranged from 5.1 to 14.3 m/s. About 61% of the cases showed abnormally high PWV values of more than 9 m/s. A total of 782 PWV examinations had been performed in the 304 autopsy cases. The average (±S.D.) and median numbers of PWV examinations per case were 2.6 (±1.9) and twice times, respectively. The largest number of examinations in one patient was 15 times. The intervals between the date of the last PWV examination and the date of death ranged from 10 days to 12.7 years. The average (±S.D.) and median intervals were 4.1 (±3.1) years and 3.5 years, respectively.

3.2. Clinical data and PWV

A positive correlation was observed between the age of the subjects at the time of the PWV examination and the PWV ($n = 3057$, $\gamma = 0.273$, $P < 0.001$). In the autopsy cases, a similar correlation between the age at death and the mean PWV was noted ($n = 304$, $\gamma = 0.250$, $P < 0.001$). When the last PWV data were applied in place of the mean PWV, weaker correlations were observed in the entire analysis. No significant sexual difference in the PWV was observed ($n = 304$, $P > 0.1$).

Histograms of the mean systolic and diastolic pressures and the mean pulse pressure showed normal distribution. The average pressures (±S.D.) were 146 (±20), 77 (±10), and 69 (±18) mmHg, respectively. A positive correlation was noted between the blood pressures and the PWV at all PWV examinations, as shown in Table 1. Similar correlations were observed between the mean blood pressure and the mean PWV in the autopsy cases.

Table 1
Correlations between blood pressure and the pulse wave velocity

	Correlation coefficients, (r)	P
All PWV examinations ($n = 3456$)		
Systolic pressure	0.478	<0.001
Diastolic pressure	0.294	<0.001
Pulse pressure	0.390	<0.001
Autopsy cases ($n = 304$)		
Mean systolic pressure	0.504	<0.001
Mean diastolic pressure	0.336	<0.001
Mean pulse pressure	0.370	<0.001

Values are Pearson's correlation coefficients between blood pressure and pulse wave velocity. PWV indicates pulse wave velocity.

Table 2
Comparison of the mean PWV and the PAI between cases with and without atherosclerosis-related diseases

Atherosclerosis-related diseases	n^a (%)	Disease	No disease	P^b
Pulse wave velocity (m/s)				
Hypertension	198 (65%)	9.89 (±1.75)	9.00 (±1.61)	<0.001
Diabetes mellitus	52 (17%)	9.80 (±1.84)	9.53 (±1.73)	n.s.
Hyperlipidemia	71 (23%)	9.57 (±1.58)	9.59 (±1.81)	n.s.
Ischemic heart disease	78 (26%)	9.71 (±1.77)	9.54 (±1.75)	n.s.
Cerebrovascular disease	109 (36%)	9.74 (±1.85)	9.49 (±1.70)	n.s.
Pathological atherosclerotic index (points)				
Hypertension	180 (65%)	4.78 (±1.42)	3.93 (±1.26)	<0.001
Diabetes mellitus	49 (18%)	5.18 (±1.32)	4.34 (±1.40)	<0.001
Hyperlipidemia	66 (24%)	4.71 (±1.57)	4.42 (±1.37)	n.s.
Ischemic heart disease	70 (25%)	5.17 (±1.39)	4.26 (±1.36)	<0.001
Cerebrovascular disease	98 (36%)	4.75 (±1.49)	4.35 (±1.37)	<0.05

Values are mean (±S.D.) of the PWV and PAI. PWV indicates pulse wave velocity; PAI, pathological atherosclerotic index; and n.s., not significant.
[a] Number of cases with an atherosclerosis-related disease, with percentages indicated in parentheses.
[b] Student's *t*-test.

A multiple regression analysis of the PWV in all the examinations ($n=3454$) showed significant contributions of systolic blood pressure ($\beta=0.448$, $P<0.0001$) and age ($\beta=0.183$, $P<0.0001$).

Underlying diseases and complications of atherosclerosis were frequently encountered, as shown in Table 2. The mean PWV was significantly different between hypertensive and normotensive cases. No significant differences of the PWV were observed in relation to other diseases.

3.3. Vascular pathology

The average atherosclerotic scores varied significantly among the individual arteries ($P<0.001$), as shown in Table 3. The scores for the aorta and arteries of the lower extremities (common iliac and femoral arteries) were high, while those for the visceral arteries (splenic and superior mesenteric arteries) were low. A majority (85%) of the cases showed moderate to severe aortic atherosclerosis. There were no significant differences in the scores between the left-sided and right-sided arteries in the case of arteries examined bilaterally (common carotid, subclavian, common iliac and external iliac arteries).

The histogram of the PAI revealed a normal distribution with a mean (±S.D.) of 4.5 (±1.4) points and a range from 1.1 to 7.9 points.

3.4. Clinical data and vascular pathology

There was a positive correlation between the age at death and the PAI ($n=275$, $\gamma=0.219$, $P<0.001$). There was no significant difference in the PAI between the two sexes ($P>0.5$). There were significantly positive correlations between the mean systolic pressure and the PAI ($\gamma=0.175$, $P<0.005$), and between the mean pulse pressure and the PAI ($\gamma=0.191$, $P<0.005$); on the other hand, there was no significant correlation between the mean diastolic pressure and the PAI ($\gamma=0.002$, $P>0.5$).

As shown in Table 2, significant differences of the mean PAI were found between cases with and without atherosclerosis-related diseases, except for the case of hyperlipidemia. Table 2 indicates that the PAI is

Table 3
Atherosclerotic score of individual arteries and its correlation with the mean PWV

Name of arteries (a.)	*n*	Atherosclerotic score	Correlation with mean PWV	*P*
Common carotid a.	301	3 (2–4)	0.286	<0.001
Subclavian a.	301	4 (2–5)	0.318	<0.001
Aorta	299	7 (6–8)	0.239	<0.005
Splenic a.	297	2 (0–5)	0.300	<0.001
Superior mesenteric a.	290	2 (0–4)	0.334	<0.001
Common iliac a.	301	8 (6–8)	0.291	<0.005
External iliac a.	301	4 (2–6)	0.248	<0.005
Left femoral a.	300	6 (4–8)	0.330	<0.001
CSI	304	7 (10–12)	0.186	<0.005
BAI	268	3.2 (1.8–4.4)	0.208	<0.001

Values in each column are number of cases examined, the median of the atherosclerotic scores with percentiles (25–75%) indicated in parentheses, Spearman's correlation coefficients (ρ) between the atherosclerotic score and the mean PWV, and the level of significance. PWV indicates pulse wave velocity; CSI, coronary stenotic index (range: 0–15); BAI, brain atherosclerotic index (range: 0–8).

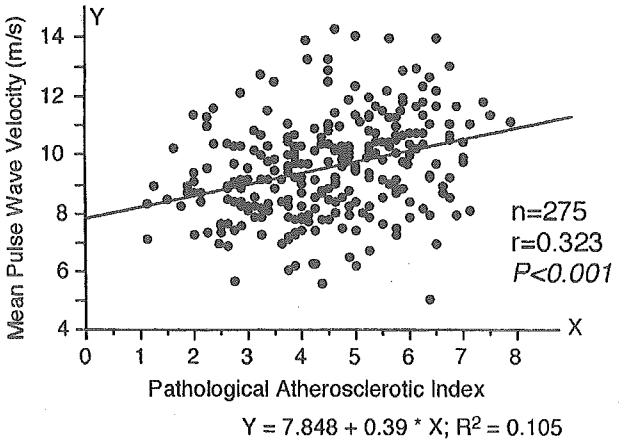

Fig. 2. Correlation between the pathological atherosclerotic index and the mean pulse wave velocity.

more related to atherosclerosis-related diseases than the PWV.

3.5. Vascular pathology and PWV

As shown in Table 3, there were positive correlations between the atherosclerotic scores of the individual arteries and the mean PWV. When the arteries with atherosclerosis more than moderate degree (≥6 points) were regarded as the atherosclerotic arteries, a significant correlation was present between the total numbers of the atherosclerotic arteries and the PWV ($\gamma = 0.335$, $P < 0.0001$). There was also a significantly correlation between the PAI and the mean PWV ($\gamma = 0.323$, $P < 0.001$), as shown in Fig. 2. Table 4 summarizes the correlations between the PAI and the mean PWV under specific conditions. In normotensive cases, a positive correlation was observed ($\rho = 0.336$, $P < 0.005$) between the PAI and the mean PWV. The Spearman's correlation coefficient was higher in the cases that underwent repeated PWV examinations ($\rho = 0.390$) than in those who underwent a single examination ($\rho = 0.312$). The correlation between the PAI and the mean PWV was studied with respect to the premortem intervals between the date of the last examination and the date of death. The Spearman's correlation coefficient between the PAI and the mean PWV was low ($\rho = 0.284$) in cases with an intermediate interval (2–4.9 years), and high ($\rho = 0.459$) in those with a long interval (≥5 years), while it was intermediate ($\rho = 0.337$) in the cases where the interval was short (<2 years). Thus, the correlation between the PAI and PWV seemed to be independent of the premortem intervals in the present autopsy cases.

Table 4
Correlations between the PAI and mean PWV

	n	Correlation coefficients (ρ)	P
All autopsy cases	275	0.353	<0.001
Blood pressure			
Normotensive	95	0.336	<0.005
Hypertensive	180	0.271	<0.001
Number of PWV examinations			
Single	124	0.312	<0.001
Multiple	151	0.390	<0.001
Premortem interval[a]			
0–1.9 years	87	0.337	<0.005
2.0–4.9	89	0.284	<0.01
≥5.0	99	0.459	<0.001

Values are Spearman's correlation coefficients (ρ) between the PAI and PWV. PAI indicates pathological atherosclerotic index; PWV, pulse wave velocity.
[a] Premortem interval between the date of the last PWV examination and the date of death.

Table 5
Multiple regression analysis of the pulse wave velocity in autopsy cases ($n = 304$)

	Standardized partial regression coefficients (β-values)	Correlation coefficients (γ-values)
Mean systolic blood pressure	0.444*	0.038
Age at death	0.154**	0.036
PAI	0.209*	0.258
Coefficient of determination (R^2)	0.331	

PAI: pathological atherosclerotic index.
* $P < 0.0001$.
** $P < 0.005$.

A "changing rate" of PWV was defined as a regression coefficient of PWV in simple regression analysis. The meta-regression analysis showed a positive correlation between the changing rate of PWV and the PAI, independent of the mean PWV values. Each 1 m/s increase of PWV per month corresponded to an increase of PAI of 0.69 points.

A multiple regression analysis was performed to determine the contributions of the major decisive factors of the PWV. Three independent factors, namely, age at death, mean systolic blood pressure and the PAI, were selected for the analysis. The result of the analysis was shown in Table 5. The standardized partial regression coefficient and correlation coefficient between the PAI and the mean PWV were 0.209 and 0.258, respectively. Thus, the PAI accounted for only 5% (=0.209 × 0.258) of the variability of the variance of the PWV.

4. Discussion

Arteriosclerosis comprises three different pathological entities: atherosclerosis of elastic or muscular arteries, Monckeberg arteriosclerosis (medial calcific sclerosis) of muscular arteries, and arteriolosclerosis. All of these entities are very common in the elderly and, in the present study, 85% of the subjects showed moderate to severe atherosclerosis of the aorta. In the early stage of atherosclerosis, the intima is involved, but the subsequent medial destruction and fibrosis

result in arterial dilatation and decrease of elasticity. Meanwhile, the PWV reflects the mechanical properties of the arterial wall, especially the amount and structure of the elastic fibers in the media, and is closely correlated with the blood pressure. The present study revealed a weak, but positive correlation between the PAI and the PWV in normotensive subjects. A changing rate of the PWV, as well as the PWV itself, was correlated with the PAI. In other words, a higher changing rate meant more severe atherosclerosis. Takahashi performed serial PWV measurements in a variety of patients and the results were consistent with ours, in that the changing rate of the PWV was especially high in cases of hypertension, ischemic heart disease and diabetes mellitus [17]. The correlation coefficient between the PAI and the PWV was higher in those cases who underwent repeated examinations than in the cases who underwent a single examination. These results led us to conclude that repeated PWV measurements could give us precise information about the severity of atherosclerosis.

The blood pressure and age of the patients are both important factors influencing the PWV. But, it is uncertain whether the high PWV values among hypertensive patients and the elderly are caused by the physiological responses to high blood pressure and the aging process, or by the concomitant atherosclerosis which is also common in these subpopulations. Multiple regression analysis in the present study showed that atherosclerosis was a more important factor influencing the PWV than the age of the patients. Earlier reports stated that aging is the dominant factor responsible for reduced arterial compliance, in other words, increases of PWV, and that the concomitant atherosclerosis is an additional factor of arterial stiffness [1,2]. The decrease and fragmentation of elastic fibers and increase of collagen fibers in the arterial wall associated with aging are considered to be the cause of the increase of PWV. Hosoda et al. reported that the elastic fiber contents of the aorta in non-atherosclerotic cases sharply decreased from 40% in neonates to 27% in the sixth decade, but it remained unchanged thereafter until the ninth decade [18]. Since the cases examined in the present study were all elderly people over the age of 67 years, Hosoda's data were not inconsistent with our results.

To the best of our knowledge, there is no report so far in English medical literature of the existence of a correlation between the PWV and the severity of atherosclerosis as examined by pathological methods. Otuska [19] performed a pathological study on this subject based on 72 autopsy examinations and reported, in a Japanese journal, the existence of a positive correlation between the PWV and pathological changes in the aorta, especially the intimal changes seen in atherosclerosis. Farrar et al. [20,21], in a series of experimental studies on non-human primates, reported that atherosclerosis caused thickening of the arterial wall and medial degeneration, which caused an increase of the PWV. He also observed that discontinuation of a diet high in fat caused regression of atheroma and decrease of the PWV values [22].

Blacher et al. [10] studied the correlations between the PWV and the severity of atherosclerosis in selected arteries in hypertensive patients. In their studies, the diagnosis of the atherosclerosis depended on clinical information and imaging techniques such as the carotid echography and abdominal CT. Our study was different from the other studies including the one by Blacher et al., in that the assessment was based on the pathological examination, which can detect the subclinical or uncomplicated atherosclerosis. They reported a good correlation between the PWV and the severity of atherosclerosis in aorta and the arteries of the lower limbs. The present study showed a relatively good correlation with the PWV in the femoral artery and a relatively weak one in the aorta.

Some limitations of our study warrant attention. As the intervals between the date of the PWV measurements and the date of death were occasionally very long, in some cases more than 5 years, the atherosclerosis might have progressed or regressed after the last examination. In the present study, however, a long interval was not associated with any decrease in the correlation coefficient between the PAI and the PWV.

In several reports, high PWV were described in the patients with hypertension, diabetes mellitus, hyperlipidemia, ischemic heart disease and cerebrovascular diseases. In contrast, the differences in the PWV were statistically significant only in hypertension in the present study. Furthermore, the correlation between PAI and PWV seems so weak, considering only 5% of the variability of PWV was explained by PAI. We frequently observed that the pathological features differ significantly from case to case among the cases with the same degree of atherosclerosis. These features included presumable important influencing factors of the PWV, such as the degree of medial destruction, the diameter of the arterial lumen, and the presence of calcification. This pathological variety may result in a low correlation between the severity of atherosclerosis and the PWV. The weak correlation might be caused by the long premortem intervals mentioned above. Since the tonometric assessment employed in this study is known to less accurate and reproducible than a newly developed oscillometric method [23]. Future autopsy study with an oscillometric PWV measurement is expected to reveal a better association between atherosclerosis and PWV.

5. Perspectives

The PWV examination has become a powerful screening tool to detect the subjects with high cardiovascular and cerebrovascular risks. The present study provides indisputable pathological evidence that the PWV correlates with the severity of aortic and systemic atherosclerosis. Meanwhile, a better association of the PAI to atherosclerosis-related diseases than that of the PWV indicated that the pathological assessment (PAI) of atherosclerosis was superior to its physiological assessment (PWV). Since pathological examinations of atherosclerosis are impossible to perform in living subjects, the development of alternative noninvasive imaging tech-

niques for morphological assessment, such as CT or MRI, is necessary and would be of great benefit in the future.

References

[1] Avolio AP, Chen SG, Wang RP, Zhang CL, Li MF, O'Rourke MF. Effects of aging on changing arterial compliance and left ventricular load in a northern Chinese urban community. Circulation 1983;68:50–8.

[2] Avolio AP, Deng FQ, Li WQ, et al. Effects of aging on arterial distensibility in populations with high and low prevalence of hypertension: comparison between urban and rural communities in China. Circulation 1985;71:202–10.

[3] Blacher J, Asmar R, Djane S, London GM, Safar ME. Aortic pulse wave velocity as a marker of cardiovascular risk in hypertensive patients. Hypertension 1999;33:1111–7.

[4] Meaume S, Benetos A, Henry OF, Rudnichi A, Safar ME. Aortic pulse wave velocity predicts cardiovascular mortality in subjects >70 years of age. Arterioscler Thromb Vasc Biol 2001;21:2046–50.

[5] Laurent S, Boutouyrie P, Asmar R, et al. Aortic stiffness is an independent predictor of all-cause and cardiovascular mortality in hypertensive patients. Hypertension 2001;37:1236–41.

[6] Boutouyrie P, Tropeano AI, Asmar R, et al. Aortic stiffness is an independent predictor of primary coronary events in hypertensive patients: a longitudinal study. Hypertension 2002;39:10–5.

[7] Wada T, Kodaira K, Fujishiro K, et al. Correlation of ultrasound-measured common carotid artery stiffness with pathological findings. Arterioscler Thromb 1994;14:479–82.

[8] Feinstein SB, Voci P, Pizzuto F. Noninvasive surrogate markers of atherosclerosis. Am J Cardiol 2002;89:31C–43C.

[9] van Popele NM, Grobbee DE, Bots ML, et al. Association between arterial stiffness and atherosclerosis: the Rotterdam Study. Stroke 2001;32:454–60.

[10] Blacher J, Fournier V, Asmar R, et al. Aortic pulse wave velocity as a marker of atherosclerosis in hypertension. Cardiovasc Rev Rep 2001;22:420–5, 431.

[11] Oda S, Matsushita S, Takahashi R, et al. Pulse wave velocity in the elderly. J Jpn Atheroscler Soc 1985;13:1231–6 [in Japanese with English abstract].

[12] Yoshimura S, Sugai J, Hashimoto H, et al. An estimation of arteriosclerosis by the measurement of pulse wave velocity and an analysis of the clinical effect of therapeutic agents on arteriosclerosis. Cor Vasa 1968;10:173–82.

[13] Gore I, Tejada C. The quantitative appraisal of atherosclerosis. Atherosclerosis 1957;33:875–85.

[14] Sugiura M, Hiraoka K, Ohkawa S. Severity of coronary sclerosis in the aged: a pathological study in 968 consecutive autopsy cases. Jpn Heart J 1976;17:471–8.

[15] Chida K, Ohkawa S, Watanabe C, Shimada H, Ohtsubo K, Sugiura M. A morphological study of the normally aging heart. Cardiovasc Pathol 1994;3:1–7.

[16] Koyama S, Saito Y, Yamanouchi H, et al. Marked decrease of intracranial atherosclerosis in contrast with unchanged coronary artery stenosis in Japan. Jpn J Geriatr 2003;40:267–73 [in Japanese with English abstract].

[17] Takahashi M. The change of pulse wave velocity with aging. J Jpn Coll Angiol 1984;24:637–43 [in Japanese].

[18] Hosoda Y, Kawano K, Yamasawa F, Ishii T, Shibata T, Inayama S. Age-dependent changes of collagen and elastin content in human aorta and pulmonary artery. Angiology 1984;35:615–21.

[19] Otsuka F. A study on relationship between pulse wave velocity of human aorta and its postmortem histo-pathology. Jikei Med J 1973;88:322–37 [in Japanese with English abstract].

[20] Farrar DJ, Green HD, Bond MG, Wagner WD, Gobbee RA. Aortic pulse wave velocity, elasticity, and composition in a non-human primate model of atherosclerosis. Circ Res 1978;43:52–62.

[21] Farrar DJ, Bond MG, Sawyer JK, Green HD. Pulse wave velocity and morphological changes associated with early atherosclerosis progression in the aortas of cynomolgus monkeys. Cardiovasc Res 1984;18:107–18.

[22] Farrar DJ, Green HD, Wagner WD, Bond MG. Reduction in pulse wave velocity and improvement of aortic distensibility accompanying regression of atherosclerosis in the rhesus monkey. Circ Res 1980;47:425–32.

[23] Munakata M, Ito N, Nunokawa T, Yoshinaga K. Utility of automated brachial ankle pulse wave velocity measurements in hypertensive patients. Am J Hypertens 2003;16:653–7.

Journal of Neuroscience Research 80:120–128 (2005)

Abnormal Accumulation of Citrullinated Proteins Catalyzed by Peptidylarginine Deiminase in Hippocampal Extracts From Patients With Alzheimer's Disease

Akihito Ishigami,[1]* Takako Ohsawa,[2] Masaharu Hiratsuka,[3] Hiromi Taguchi,[1] Saori Kobayashi,[1] Yuko Saito,[4] Shigeo Murayama,[4] Hiroaki Asaga,[5] Tosifusa Toda,[6] Narimichi Kimura,[2] and Naoki Maruyama[1]

[1]Department of Molecular Pathology, Tokyo Metropolitan Institute of Gerontology, Itabashi-ku, Tokyo, Japan
[2]Cellular Signaling Research Group, Tokyo Metropolitan Institute of Gerontology, Itabashi-ku, Tokyo, Japan
[3]Department of Molecular and Cell Genetics, Graduate School of Medical Science, Tottori University, Tottori-shi, Tottori, Japan
[4]Department of Neuropathology, Tokyo Metropolitan Institute of Gerontology, Itabashi-ku, Tokyo, Japan
[5]Biological Science Laboratory, Meiji University, Suginami-ku, Tokyo, Japan
[6]Proteomics Collaboration Research Group, Tokyo Metropolitan Institute of Gerontology, Itabashi-ku, Tokyo, Japan

Citrullinated proteins are the products of a posttranslational process in which arginine residues undergo modification into citrulline residues when catalyzed by peptidylarginine deiminases (PADs) in a calcium ion-dependent manner. In our previous report, PAD2 expressed mainly in the rat cerebrum became activated early in the neurodegenerative process. To elucidate the involvement of protein citrullination in human neuronal degeneration, we examined whether citrullinated proteins are produced during Alzheimer's disease (AD). By Western blot analysis with antimodified citrulline antibody, citrullinated proteins of varied molecular weights were detected in hippocampal tissues from patients with AD but not normal humans. Two of the citrullinated proteins were identified as vimentin and glial fibrillary acidic protein (GFAP) by using two-dimensional gel electrophoresis and MALDI-TOF mass spectrometry. Interestingly, PAD2 was detected in hippocampal extracts from AD and normal brains, but the amount of PAD2 in the AD tissue was markedly greater. Histochemical analysis revealed citrullinated proteins throughout the hippocampus, especially in the dentate gyrus and stratum radiatum of CA1 and CA2 areas. However, no citrullinated proteins were detected in the normal hippocampus. PAD2 immunoreactivity was also ubiquitous throughout both the AD and the normal hippocampal areas. PAD2 enrichment coincided well with citrullinated protein positivity. Double immunofluorescence staining revealed that citrullinated protein- and PAD2-positive cells also coincided with GFAP-positive cells, but not all GFAP-positive cells were positive for PAD2. As with GFAP, which is an astrocyte-specific marker protein, PAD2 is distributed mainly in astrocytes. These collective results, the abnormal accumulation of citrullinated proteins and abnormal activation of PAD2 in hippocampi of patients with AD, strongly suggest that PAD has an important role in the onset and progression of AD and that citrullinated proteins may become a useful marker for human neurodegenerative diseases. © 2005 Wiley-Liss, Inc.

Key words: Alzheimer's disease; astrocyte; citrulline; glial fibrillary acidic protein; PAD; vimentin

Numerous proteases and posttranslational modification enzymes participate in neurodegeneration, such as that in patients with Alzheimer's disease (AD) and Parkinson's disease (Keller et al., 2000; Maccioni et al., 2001). However, little attention has been paid to one such group of agents, peptidylarginine deiminases (PADs; EC 3.5.3.15; Rogers and Simmonds, 1958; Kubilus et al., 1980; Kubilus and Baden, 1983; Ishigami et al., 1996). PADs are a group of posttranslational modification enzymes that citrullinate (deiminate) protein arginine residues in a calcium ion-dependent manner, yielding citrulline residues. Enzymatic citrullination abolishes positive charges of native protein molecules, inevitably causing significant alterations in their structure and functions (Lamensa and Moscarello, 1993; Imparl et al., 1995; Tarcsa et al., 1996). In mammalian tissues, PADs are found as

*Correspondence to: Akihito Ishigami, PhD, Department of Molecular Pathology, Tokyo Metropolitan Institute of Gerontology, 35-2 Sakae-cho, Itabashi-ku, Tokyo 173-0015, Japan. E-mail: ishigami@tmig.or.jp

Received 4 October 2004; Revised 22 December 2004; Accepted 4 January 2005

Published online 9 February 2005 in Wiley InterScience (www.interscience.wiley.com). DOI: 10.1002/jnr.20431

TABLE I. Subject Demographic Data*

	Age (years)	PMI (hr)	Gender	BW (g)	Braak stage NFT	Braak stage SP
AD	84.5 ± 1.4	7.9 ± 2.1	3 M/7 F	1,104 ± 99	VI (10)	C (10)
Control	79.2 ± 1.6	6.5 ± 2.4	5 M/4 F	1,226 ± 31	I (9)	0 (6), A (3)

*Data are expressed as mean ± SEM. Parentheses indicated the number of subject. PMI, post-mortem interval; BW, brain weight; NFT, neurofibrillary tangle; SP, senile plaque; AD, Alzheimer disease.

five different isoforms (i.e, types 1–4, 6), which differ in specificity for various synthetic substrates, such as benzoyl-L-arginine ethyl ester and benzoyl-L-arginine, and in tissue distribution (Watanabe et al., 1988; Terakawa et al., 1991; Chavanas et al., 2004). All these isoforms display nearly identical amino acid sequences (Watanabe and Senshu, 1989; Tsuchida et al., 1993; Nishijyo et al., 1997; Ishigami et al., 1998; Nakashima et al., 1999; Rusd et al., 1999), but they appear to be dissimilar in tissue-specific expression, as evidenced by reverse transcriptase-polymerase chain reaction (Ishigami et al., 2001). Among them, only PAD2 has been proved to be an occupant of the rat central nervous system (Kubilus and Baden, 1983; Watanabe et al., 1988; Terakawa et al., 1991). Immunocytochemical studies have localized PAD2 in glial cells, especially astrocytes (Vincent et al., 1992; Asaga and Ishigami, 2000, 2001), microglial cells (Vincent et al., 1992; Asaga et al., 2002), and oligodendrocytes (Akiyama et al., 1999). Because citrullinated proteins were rarely located in the enzyme-positive glial cells examined with our sensitive detection method (Senshu et al., 1992), we assumed that PAD2 is normally inactive (Asaga and Ishigami, 2000, 2001; Asaga et al., 2002). However, glial fibrillary acidic protein (GFAP) was highly susceptible to the attack of PAD2 in excised rat brains deliberately left at room temperature (Asaga and Senshu, 1993). These findings provided a clue that PAD2 normally remains inactive but becomes active and citrullinates cellular proteins when the intracellular calcium balance is upset during neurodegenerative changes.

The pathological presentation of AD involves the selective death of pyramidal neurons and an accumulation of two main abnormal protein aggregates, senile plaques (SPs) and neurofibrillary tangles (NFTs; Katzman, 1986; Smith, 1998). Although NFTs and SPs are found in many areas of the cerebrum, they are concentrated mainly in the hippocampus and cerebral cortex. The former site actually appears to be more important, since pathological indices are first localized in that region (Maccioni et al., 2001). Our previous report indicates that levels of PAD2 are more than threefold higher in the hippocampus than in the cortex of rat brains (Asaga and Ishigami, 2000). Moreover, PAD2 activates and citrullinates various cerebral proteins under hypoxic conditions (Asaga and Ishigami, 2000) and during kainic acid-evoked neurodegeneration (Asaga and Ishigami, 2001; Asaga et al., 2002), suggesting the involvement of protein citrullination in neurodegenerative processes. The present study was therefore designed to test the hypothesis that PAD2 plays a role in AD and that citrullinated proteins are active participants in the neurodegenerative process, particularly in the hippocampus.

MATERIALS AND METHODS

Human Subjects

Brain specimens used in this study were removed at autopsy from 10 patients with AD (seven women and three men) and nine (four women and five men) normal subjects. The subjects' demographic data are summarized in Table I. Specimens were taken from the hippocampus and divided into two parts. One part was fixed with 4% paraformaldehyde and processed for paraffin embedding. Another part was immediately frozen in dry ice. All AD patients met accepted criteria for the neuropathologic diagnosis of AD based on the National Institute of Aging (NIA)-Reagan Institute Criteria for the Neuropathological Diagnosis of AD (1997), combining abundant neuritic plaques in the neocortex (definite AD with Consortium to Establish a Registry for AD Criteria) and a profusion of NFTs in the limbic and neocortical areas (Braak and Braak stage VI). Normal subjects used as controls were individuals with no history of dementia or other neurologic disorders. Neuropathologic evaluation of control brains revealed only age-associated gross and histopathologic alterations (Braak and Braak NFT stage I and senile plaque stage 0 or A). The human studies were approved by the Tokyo Metropolitan Institute of Gerontology (TMIG) Review Boards.

Preparation of Tissue Samples

Frozen hippocampi of AD and control subjects' brains were homogenized in a lysis buffer (0.01 M Tris-HCl, pH 7.6, 1 mM phenylmethylsulfonyl fluoride, 0.1% NP-40) with a Polytron homogenizer. For sodium dodecyl sulfate-polyacrylamide gel electrophoresis (SDS-PAGE), an aliquot of the homogenates was mixed with an equal volume of 0.125 M Tris-HCl, pH 6.8, 4% SDS, 20% glycerol, 10% 2-mercaptoethanol, and 0.005% bromophenol blue (sample buffer) and heated in boiling water for 5 min. The protein content of cell homogenates was measured by the method of Lowry et al. (1951) with bovine serum albumin as a standard.

Detection of Citrullinated Proteins

Citrullinated proteins were detected by Western blotting as described previously (Senshu et al., 1992). Briefly, equal amounts of protein (10 μg/lane) were separated by SDS-PAGE on vertical slab 10% acrylamide gels (1 mm × 9 cm) by the method of Laemmli (1970). Proteins were then electrophoretically transferred from acrylamide gels onto a membrane of poly-

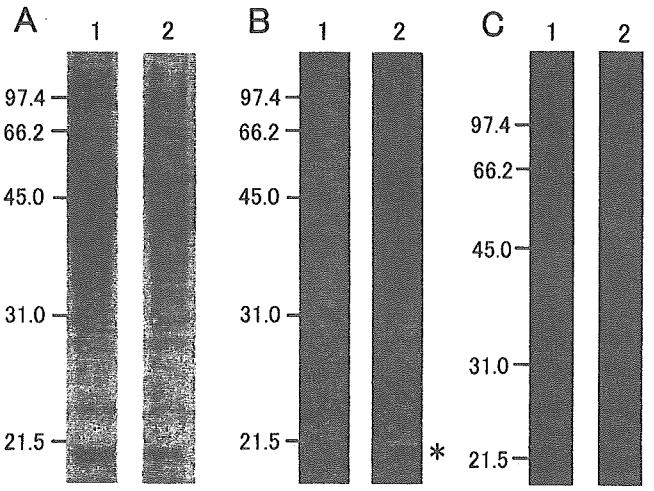

Fig. 1. Western blot analysis of citrullinated proteins and PAD2 in the hippocampus of AD and control brain. Tissue homogenates (10 μg) were separated by SDS-PAGE and transferred to a PVDF membrane. **A:** Typical protein profiles detected by amido black staining. **B:** Citrullinated protein profiles detected as described in Materials and Methods. **C:** Immunoreactive PAD2 profiles. Lane 1, age-matched control; lane 2, AD. Asterisks indicate the citrullinated MBP.

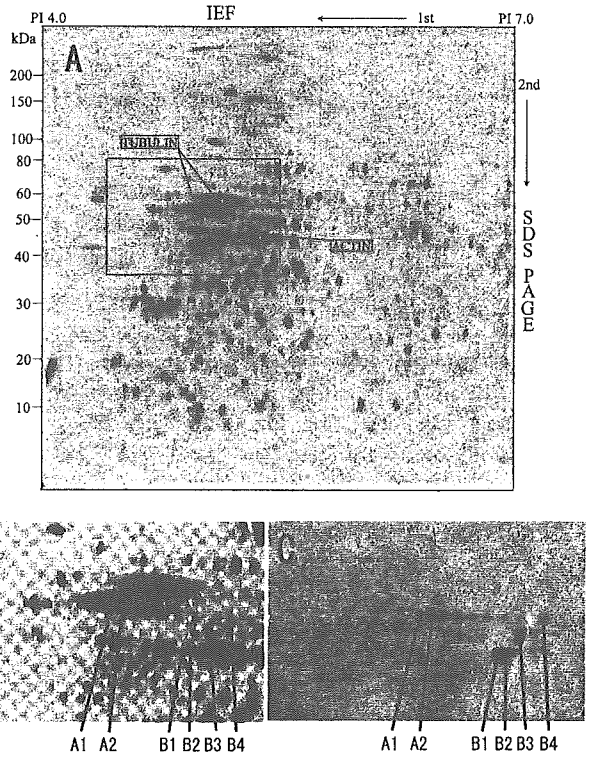

Fig. 2. Proteome analysis of citrullinated proteins in the hippocampus of AD brain. **A:** Two-dimensional protein profiles of the AD hippocampus. Proteins were separated on the basis of pI (x-axis) and molecular mass (y-axis). Spots were visualized with Sypro Ruby gel staining. IEF, isoelectric focusing. Tubulin and actin were identified by peptide mass fingerprinting and a subsequent database search. **B:** Enlarged proteins of AD hippocampus from 2-DE gels indicated as a rectangular area in A. **C:** Western blot analysis of citrullinated proteins from 2-DE gels indicated as rectangular area in A. Numbered spots were identified by mass spectrometry.

vinylidene difluoride (PVDF; Millipore, Billerica, MA) by the method of Towbin et al. (1979). Citrulline residues on the membrane were modified by overnight incubation at 37°C in modification medium [1 volume of 1% diacetyl monoxime/0.5% antipyrine/1 N acetic acid, and two volumes of a mixture of 85% H_3PO_4/98% H_2SO_4/H_2O (20/25/55) containing 0.025% $FeCl_3$]. The membrane was then incubated successively with antimodified citrulline IgG antibody produced in a rabbit and with purified (Senshu et al., 1992), horseradish peroxidase-labeled goat anti-rabbit IgG (Bio-Rad, Hercules, CA). Chemiluminescence signals were detected on Kodak XAR films with ECL Western Blotting Detection Reagents (Amersham Bioscience, Piscataway, NJ).

Two-Dimensional Gel Electrophoresis and Proteome Analysis

Protein extraction and two-dimensional gel electrophoresis (2-DE) were performed as reported previously (Toda et al., 1998; see also http://proteome.tmig.or.jp/2D/2DEmethod.html). Briefly, 100 mg of tissue sample were crushed in liquid nitrogen and lysed with 300 μl of 5 M urea, 2 M thiourea, 2% CHAPS, 2% SB3-10, 1% Pharmalyte (pH 3–10; Amersham Bioscience), 1% dithiothreitol (DTT), and 1% proteinase inhibitor cocktail (Sigma-Aldrich, St. Louis, MO) with sonication. One hundred micrograms of protein were loaded onto gel strips with an immobilized pH gradient (pH 4–7; 18 cm; Amersham Biosciences), and isoelectric focusing was performed on a CoolPhoreStar model 3610 (Anatech, Tokyo, Japan). After isoelectric focusing, strips were equilibrated with 50 mM Tris-HCl, pH 6.8, 6 M urea, 2 M thiourea, 2% SDS, 30% glycerol, and 1% DTT for 30 min and then with the same solution containing 4% iodoacetamide instead of DTT for 30 min. Each equilibrated strip was mounted on a 7.5% SDS-polyacrylamide gel and fixed with shark-tooth combs. SDS-PAGE was performed on a vertical format using a Tricine buffer system. After second-dimension electrophoresis, gels were fixed in 10% methanol and 6% acetic acid for 30 min, and protein spots were visualized by Sypro Ruby (Molecular Probes, Eugene, OR) staining, following the manufacturer's recommendations.

A square (8 × 8 cm) containing tubulin was cut off from the gel slab and then applied to Western blots to detect the citrullinated proteins according to the method described above, because these citrullinated proteins were previously detected at the same position of tubulin on 2-DE using minislab gel (8 × 8 cm). At this time, the citrullinated proteins were detected by using the highly sensitive reagent ECL Advance (Amersham Bioscience). Thereafter, the protein spots visualized with Cypro Ruby and matched with the citrullinated proteins were excised with a ProteomeWorks Spot Cutter (Bio-Rad) followed by in-gel digestion with trypsin according to the manufacturer's specifications. The digested peptide was directly mixed with an equal volume of 10 mg/ml α-cyano-4-hydroxycinnamic acid, and peptide mass spectra were obtained on an AXIMA-CFR MALDI-TOF-MASS (Shimadzu, Kyoto, Japan) platform. Peptide mass mapping was

TABLE II. Proteins Identified From 2-DE Gels of AD Hippocampus by MALDI-TOF Mass Spectrometry

Spot no.[a]	Protein	Probability	Sequence coverage (%)	NCBI accession Nos.	Theoretical value		Experimental value	
					pI	kDa	pI	kDa
A1	Vimentin	3.8E+02	68	CAA39600	5.1	53.7	5.1	49.2
A2	Vimentin	4.3E+02	71	CAA39600	5.1	53.7	5.1	49.1
B1	GFAP	3.1E+02	53	NP_002046	5.4	49.9	5.2	43.5
B2	GFAP	3.3E+02	57	NP_002046	5.4	49.9	5.2	44.8
B3	GFAP	3.2E+02	55	NP_002046	5.4	49.9	5.3	47.4
B4	GFAP	3.3E+02	60	NP_002046	5.4	49.9	5.3	49.9

[a]The numbering and lettering corresponding to the 2-DE gets image shown in Figure 2A.

performed by using Mascot Search (Matrix Science Ltd., London, United Kingdom).

Immunohistochemistry

The paraffin-embedded sections (6-μm-thick) of AD and control hippocampi were deparaffinized, rehydrated, and pretreated by heating in a microwave oven for 10 min in citrate buffer. Citrullinated proteins were detected as described previously (Ohsawa et al., 2001; Ishigami et al., 2002a). Briefly, sections were postfixed with 4% paraformaldehyde and 2.5% glutaraldehyde, and then they were incubated in the modification medium at 37°C for 3 hr to modify citrulline residues in situ. Immunostaining of citrullinated proteins was performed with antimodified citrulline IgG and the Vectastain Elite ABC kit (Vector Laboratories, Burlingame, CA) using 3,3′-diaminobenzidine as a chromogenic substrate. Human PAD2 and GFAP were stained with rabbit anti-human PAD2 prepared as described previously (Ishigami et al., 2002b) and monoclonal antibodies to GFAP (Sigma-Aldrich), respectively. Sections were also subjected to hematoxylin staining for histological examinations. To evaluate the degree of citrullinated protein and PAD2 immunoreactivity, we used a scoring system, in which immunoreactivity was arbitrarily defined from grade 0 (no immunoreactivity detected) to grade 4 (the most intensive immunoreactivity detected). The scores obtained from 10 AD and nine control subjects were then averaged.

The citrullinated proteins, human PAD2 and GFAP, were detected with immunofluorescent labeling and confocal microscopy (LSM-510 laser scanning microscope; Carl Zeiss, Oberkochen, Germany). Primary antibodies were visualized with Alexa Fluor 488 goat anti-rabbit IgG and Alexa Fluor 594 goat anti-mouse IgG (Molecular Probes).

Statistical Analysis

The results are expressed as the mean ± SEM. The probability of statistical differences between experimental groups was determined by a Student's *t*-test, as indicated.

RESULTS

Identification and Characterization of Citrullinated Proteins in the Hippocampi of AD Patients and Normal Controls

Figure 1A shows total proteins in hippocampal extracts from brains of AD and normal individuals in which amido black staining delineated obviously different profiles. In particular, the protein bands between 30 and 50 kDa were notably smaller in the AD hippocampal extracts. Moreover, the citrullinated protein profile from AD hippocampal samples manifested species not detected in those from normal brains (Fig. 1B) as judged by the procedures described in Materials and Methods. In particular, a band migrating at approximately 20 kDa, which was previously shown to be myelin basic protein (MBP) in cultured oligodendrocytes (Akiyama et al., 1999), was present in relatively large quantities in the AD hippocampus but essentially undetectable in this region from normal brains. We confirmed the identity of this protein by immunoprecipitation using specific MBP antiserum (data not shown). Western blots of PAD2 revealed a single band migrating at approximately 75 kDa in hippocampal extracts from both normal and AD brains (Fig. 1C).

AD hippocampal proteins were further characterized by 2-DE (Fig. 2A). Because citrullinated proteins were detected in abundance migrating over 35 kDa, as shown in Figure 1B, the gel region outlined in Figure 2A was cut out (Fig. 2B), and the citrullinated proteins were subjected to Western blotting for identification. Figure 2C shows several of the AD hippocampal citrullinated proteins detected and identification of these proteins by peptide mass fingerprinting and a subsequent database search. These methods identified vimentin as proteins A1 and A2 and GFAP as proteins B1, B2, B3, and B4 (Table II). Some citrullinated proteins were visible throughout the gel (Fig. 2A), even outside the region cut out (data not shown).

Immunohistochemical Localization of Citrullinated Proteins and PAD2 in Hippocampal Regions and Cell Type

Figure 3A shows the regional localization of citrullinated proteins in the hippocampus of an AD brain. Citrullinated proteins were detected throughout the hippocampus, especially in the conjugation region between molecular layers of hippocampus and dentate gyrus as well as polymorphic layers of dentate gyrus and stratum radiatum of CA1 and CA2 areas. No such proteins were found in the granular layer of the dentate gyrus. Moreover, no citrullinated proteins at all were detected in a normal hippocampus (Fig. 3B). A scoring system adopted to evaluate the degree of citrullinated protein immunoreactivity in the hippocampus then revealed significantly greater immunoreactivity in the AD hippocampus than in its normal counterpart (Fig. 4A). In contrast, PAD2 immunoreactivity was detect-

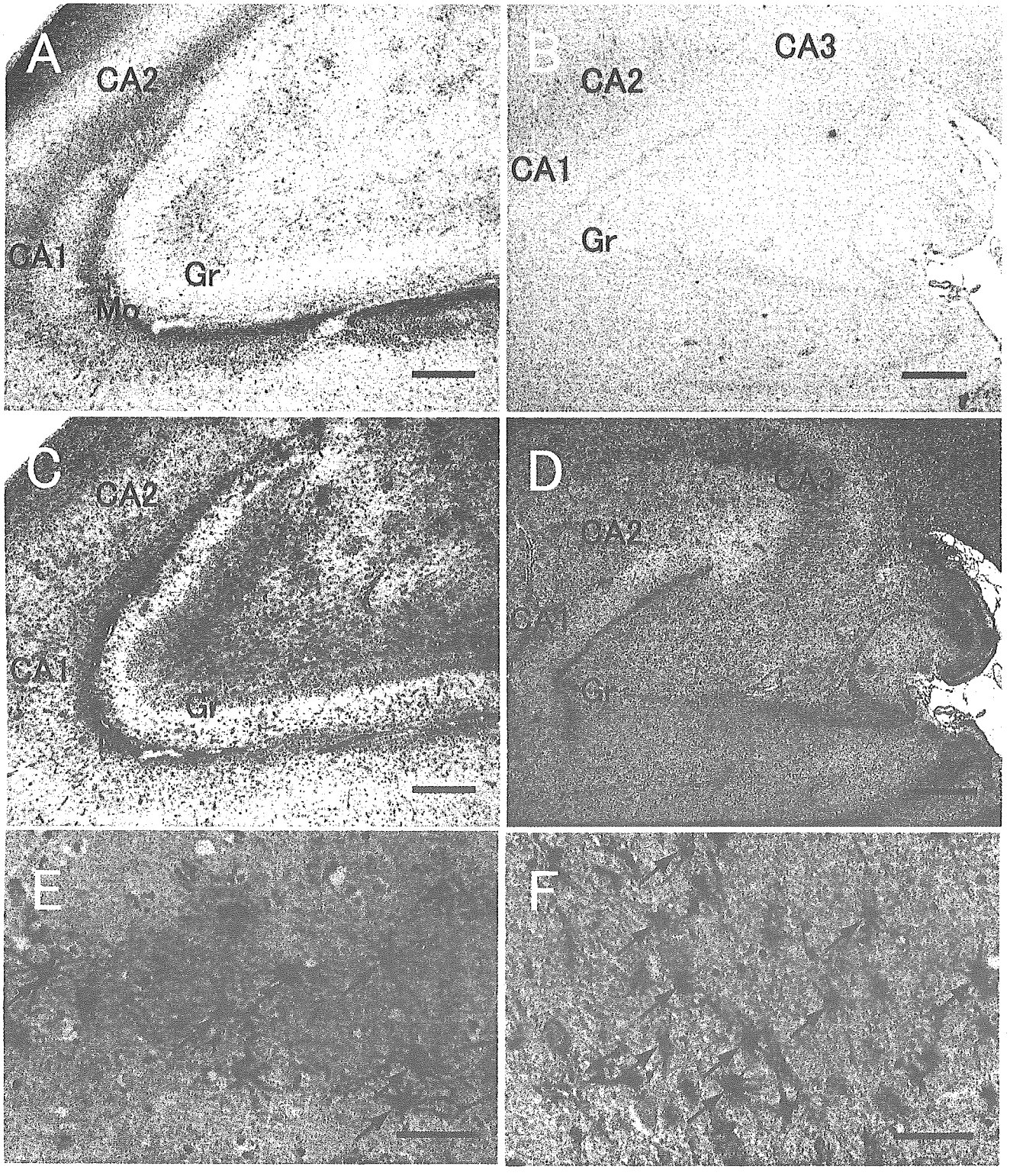

Fig. 3. Immunohistochemical staining of citrullinated proteins and PAD2. Hippocampal sections from AD (**A,C**) and control (**B,D**) brains were stained for citrullinated proteins (A,B) and PAD2 (C,D) as described in Materials and Methods. **E:** Higher magnification of A. Arrows indicate the citrullinated protein-positive cells. **F:** Higher magnification of C. Arrows indicate the PAD2-positive cells. Gr, granule cell layer; Mo, molecular cell layer. Scale bars = 500 μm in A–D, 50 μm in E,F.

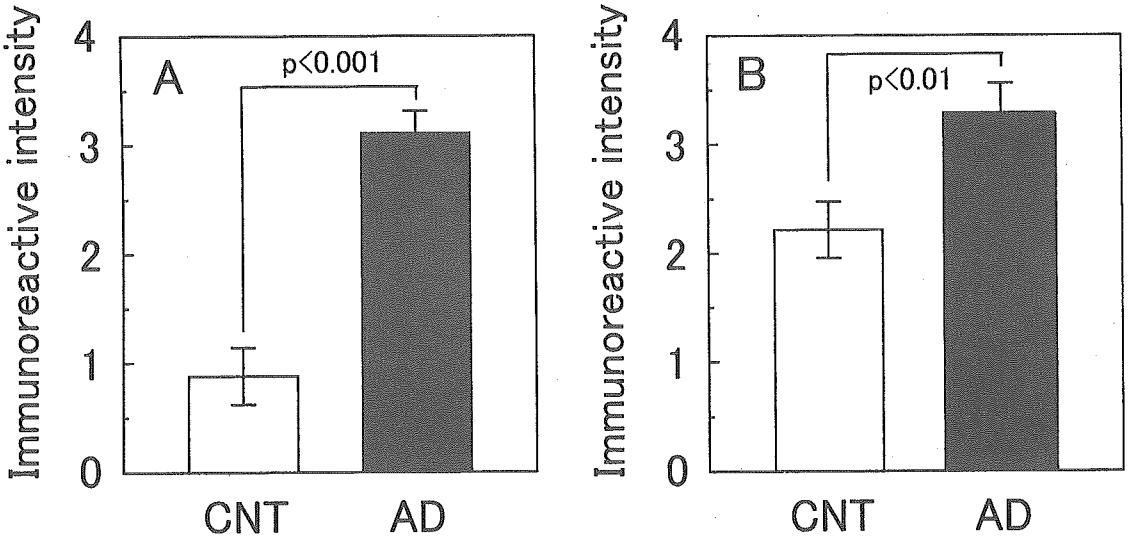

Fig. 4. Immunoreactive intensity of citrullinated proteins and PAD2 in the hippocampi of AD and control brains. The immunoreactivity of citrullinated proteins (**A**) and PAD2 (**B**) in the hippocampus was graded (grade 0 to 4) as described in Materials and Methods. Values are expressed as means ± SEM of 10 AD and nine control subjects. Data were compared by Student's *t*-test.

able all through the hippocampus, both in the AD and in normal brain, but not in the granular layer of the dentate gyrus (Fig. 3C,D). A scoring system adopted to evaluate the degree of PAD2 immunoreactivity in the hippocampus revealed significantly greater immunoreactivity in the AD hippocampus than in its normal counterpart (Fig. 4B). The PAD2-enriched region coincided well with the citrullinated protein-positive regions (Fig. 3A,C). At higher microscopic magnification in the polymorphic layer of dentate gyrus, figures of citrullinated protein-positive cells and PAD2-positive cells were apparent as astrocyte-like cells (Fig. 3E,F). To confirm whether these citrullinated protein- and PAD2-positive cells were astrocytes, we performed double-immunofluorescence staining for citrullinated protein or PAD2 and GFAP, which is an astrocyte-specific marker protein, followed by confocal microscopy (Fig. 5). GFAP-positive fluorescence signals clearly coincided with citrullinated protein-positive signals (Fig. 5A–C) as well as PAD2-positive signals (Fig. 5D–F). Almost all GFAP-positive cells showed immunoreactivity for PAD2, despite a few exceptions. Thus, PAD2 was distributed mainly in astrocytes.

DISCUSSION

We report here, for the first time, the abnormal accumulation of citrullinated proteins and abnormal activation of PAD2 in brain extracts from patients with AD. Citrullinated proteins were barely detectable in normal human brain extracts, although PAD2 was almost universally present.

Previously, we found similar results in the normal rat brain (Asaga and Ishigami, 2000, 2001). Additionally, physiologic insults such as hypoxia and kainic acid administration also resulted in the appearance of citrullinated proteins (Asaga and Ishigami, 2000, 2001; Asaga et al., 2002). PAD2 was present in the rat cerebrum and especially enriched in the dentate gyrus and stratum radiatum of hippocampus, the amygdala, the hypothalamus, and the cortex, but few or no citrullinated proteins were detected in those regions. Under hypoxic conditions (Asaga and Ishigami, 2000) and during kainic acid-evoked neurodegeneration (Asaga and Ishigami, 2001; Asaga et al., 2002), PAD2 became activated in regions undergoing neurodegeneration and functioned to citrullinate various cerebral proteins, indicating the involvement of protein citrullination in neurodegenerative processes. We are convinced that these past and present results confirm the involvement of protein citrullination in human neurodegenerative disease.

In the present study, Western blot analysis revealed numerous citrullinated proteins in the AD hippocampus. We identified citrullinated vimentin and GFAP, which were shown as several independent spots by 2-DE and proteomic analysis (Fig. 2C, Table II). Because protein citrullination results in a decrease in the net positive charge of proteins, each spot must be shown as several pI values with different degrees of citrullination resulting in neutralization of proteins. In the epidermis of mice, we previously identified citrullinated cytokeratins and filaggrin as several independent spots separable by 2-DE and detected by Western blotting (Senshu et al., 1995, 1999). Citrullination of cytokeratins and filaggrin occurs during the latest stages of epidermal differentiation and is thought to play a key role in the cornification process (Senshu et al., 1995). Although citrullination of vimentin and GFAP seems to be much more specific than that of other intracellular proteins, it is still unclear whether citrullination of vimentin and GFAP has physiologically